This article has been accepted for publication in a future issue of this journal, but has not been fully edited. Content may change prior to final publication. Citation information: DOI 10.1109/TIM.2019.2918372, IEEE Transactions on Instrumentation and Measurement

A CMOS Receiver–TDC Chip Set for Accurate Pulsed TOF Laser Ranging

Sami Kurtti, Jussi-Pekka Jansson and Juha Kostamovaara, Senior *Member, IEEE*

***Abstract*— An integrated receiver-TDC (time-to-digital converter) chip set is developed for pulsed time-of-flight (TOF) laser rangefinding. The receiver detects the current pulse from the optical detector and produces a timing mark for the TDC. The receiver uses time mode walk error compensation scheme achieving <+/-2.5 mm residual timing walk error within a dynamic range of ~1:40,000. The multi-channel TDC measures the time position, width and rise time of the echo pulses simultaneously with ~ 10 picosecond (ps) precision. Both chips are manufactured in 0.35-µm complementary metal-oxide semiconductor (CMOS) technology. The functionality of the chip set was demonstrated in a laser radar platform using 12 W and 3-ns optical pulses produced by a laser diode. A measurement accuracy of ~+/-3 mm was achieved with non-cooperative targets at a distance range of a few tens of metres within an amplitude range of received echoes of 1:40,000.**

***Index Terms*—Pulsed time-of-flight, Laser rangefinder, Laser radar receiver, Time-to-digital converter, lidar, Timing discrimination**

I. Introduction

LASER radars are commonly used for distance measurement applications in geodesy and forestry, and also in industrial applications such as the measurement of level heights in silos and containers and the measurement of the large-scale geometry of natural objects [1]–[3]. Laser ranging is usually based on time-of-flight (TOF) techniques, in which the transit time of a laser pulse or the phase shift of an amplitude-modulated continuous-wave (CW) laser signal introduced by the finite travelling time (Δt) of the signal transmitted to the target and back to the receiver is measured. Because the velocity of light (c) is known and is relatively stable under varying environmental conditions, the distance from the target (R) can be calculated using the measured time interval (Δt) or phase shift.

CW modulation-based phase comparison techniques result in relatively simple electronic realizations, but suffer from a tradeoff between the precision of the result and its ambiguity. A high precision necessitates the use of a high modulation frequency (e.g. 100 MHz), which yields a relatively short non-ambiguous measurement range. This range can be extended by using several modulation frequencies,— but at the expense of a longer measurement time and more complex realization [4]–[7]. The presence of several targets within the transmitter illumination is also an issue for CW phase-comparison laser radar techniques.

On the other hand, the pulsed TOF principle allows the obtaining of a broad unambiguous measurement range limited by the transmitter pulsing frequency (e.g. 100 kHz corresponds to ~1 km) and high precision with a high measurement speed, as a measurement based on a single transmitted pulse typically gives only centimetre-level precision [5], [8]. With regard to electrical realization, however, the pulsed TOF principle is demanding, requiring the processing of nanosecond-scale optical and electrical pulses with picosecond precision.

Pulsed TOF laser radar techniques have recently shown great potential in two-dimensional (2-D) and three-dimensional (3-D) range imaging, i.e. in environment perception systems which have applications in electrically assisted driving and in the control of machines used in the construction industry, farming and forestry (e.g. excavators, bulldozers, wood processors). Other obvious potential application areas are drones and robots [9]–[11]. One successful realization architecture uses a multi-channel spinning radar unit that can simultaneously measure distances on several (e.g., 64) vertical planes [9], [10]. In 3-D range imagers, especially when aiming at a solid-state approach using multiple detector elements (i.e. laser scanning without moving parts), miniaturization of the measurement electronics is important in order to be able to reduce the size and power consumption of the system.

The targets in laser radar applications are typically non-cooperative (Lambertian type), and the measurement range is typically from a few tens of metres up to ~100 m, while the required single-shot precision is at the centimetre level. This performance level can be achieved with laser pulses having a peak power and pulse width of >10 W and 3…5 ns, respectively, as explained in detail below. Pulses of this kind can be produced using a semiconductor laser diode (LD)-based transmitter, while the typical realization of the receiver part includes an avalanche photodiode (APD) optical detector, a low-noise pre-amplifier, post-amplifiers and a multi-bit analogue-to-digital (AD) converter, as shown in Fig. 1.

Since nanosecond-scale pulses are used, the output of the

Manuscript received xxx. This work was supported financially by the Academy of Finland (Centre of Excellence in Laser Scanning Research, contract no. 172196, and contracts nos. 255359, 263705 and 251571), which are gratefully acknowledged.

The authors are with the Circuit and Systems Research Unit, University of Oulu, 90014, Finland (email: sami.kurtti@oulu.fi, jussi.jansson@oulu.fi, juha.kostamovaara@oulu.fi).

This article has been accepted for publication in a future issue of this journal, but has not been fully edited. Content may change prior to final publication. Citation information: DOI 10.1109/TIM.2019.2918372, IEEE Transactions on Instrumentation and Measurement

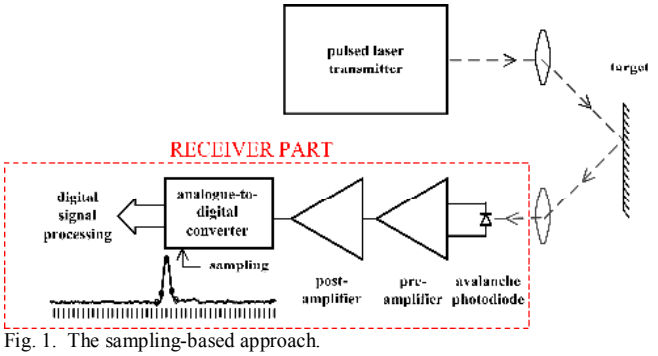

Fig. 1. The sampling-based approach.

receiver should be sampled at a relatively high rate, e.g. >500 mega samples per second, in the sampling-based receiver architecture, shown in Fig. 1. Now, a full waveform analysis can be carried out (digital signal processing, DSP). However, the high sampling rate and the need for a multi-bit AD converter will also increase the power consumption (W-range), which is a particularly serious issue in the multi-channel realizations that are especially needed in a solid-state laser scanning architecture [3].

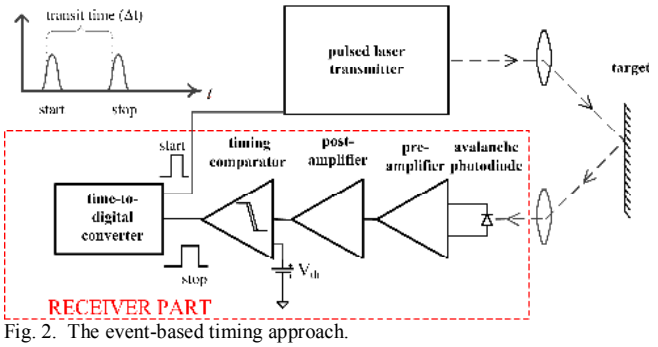

Fig. 2. The event-based timing approach.

In another receiver architecture (the event-based timing approach), which is adopted and used here, the AD converter is replaced with a non-clocked timing comparator and a time-to-digital converter (TDC), as shown in Fig. 2. The timing comparator is triggered only when the received pulse exceeds a predetermined threshold, which is defined by the noise level of the receiver and the set false-alarm rate [1], [8], [12]. The TDC is then used for direct measurements of the time interval between the emitted and received optical pulses. As a result, no continuous sampling of the receiver channel is used, which will substantially reduce the power consumption of the receiver. On the other hand, because accurate samples of the received echo pulse waveform (envelope) are not available, the variation in the amplitude of the echo due to the varying distance (~$1/R^2$), orientation and reflection properties of the objects [13] may introduce a timing accuracy problem (timing-walk error). An example of the walk error generation in timing discrimination is shown in Fig. 3 (a). The variation in the amplitude of the echo pulses causes systematic timing error (walk error) to the measured Δt and it is therefore seen in the calculated distance result ($\Delta R = c * \Delta t/2$).

The timing-walk error is produced by the dependence of the timing moment on the amplitude of the received echo signal. In simple threshold detection, the error can reach a few

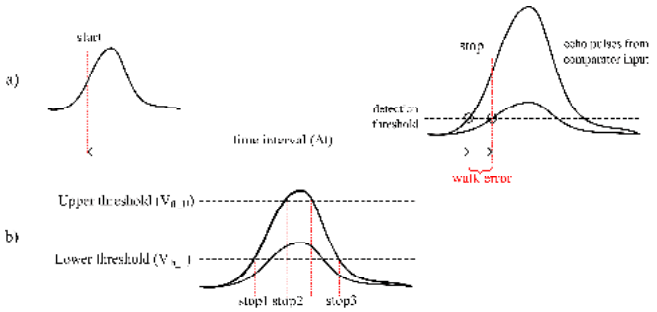

Fig. 3. (a) Timing walk-error in a leading-edge timing discriminator, (b) timing discrimination-based leading detection employing multiple thresholds (V_{th_L} and V_{th_U}).

nanoseconds (67 ps in time corresponds to 1 cm in distance) and is thus a serious issue with regard to the accuracy of the laser radar system [14]. This situation is complicated by the fact that the linear pulse amplitude range of the receiver channel as realized in modern integrated-circuit (IC) technologies is typically narrow (~1:100) as a result of the low supply voltage and the receiver sensitivity optimization [14]. Thus, to accurately discriminate the timing moment from the input signal echo by applying known linear timing discrimination techniques (e.g. zero-crossing detection or constant-fraction techniques), an automatic gain-control unit at the input to the preamplifier and/or control of the transmitted optical power would be needed. These solutions, however, may result in a mechanically bulky realization (e.g. an optical neutral density (ND) filter with varying transmittance), or else they may restrict the dynamic range owing to the varying electric group delay in the electronic gain control [15].

Another solution which is pursued here is that other time-domain parameters are measured from the received echo in addition to simple threshold detection and measurement of the corresponding time interval (start–stop). The width of the echo pulse, for example, obviously correlates with the echo amplitude; i.e. a higher amplitude corresponds to a wider received echo at a constant threshold level. Importantly, this holds good even in the case where the receiver is clamped at its maximum output amplitude level (extending the applicability of the method beyond the linear dynamic range of the receiver). In addition, another detection threshold (V_{th_U}) can be used, allowing characterization of the slew rate of the echo signal (which also correlates with the echo amplitude) as shown in Fig. 3(b). This additional timing information can then be used to compensate for the timing-walk error, as explained in detail in Section II, or even to determine the amplitude of the echo if this information is important in the specific application. For the time interval measurement a high-precision multi-channel TDC (time-to-digital converter) is also needed, enabling measurement of several time domain parameters simultaneously from a single echo pulse.

In this work a CMOS receiver–TDC chip set was developed that implements the receiver path of a pulsed TOF laser radar in accordance with the event-based timing approach and time domain walk error compensation strategy described above. The input to the chip set is the signal current from the APD, and the

This article has been accepted for publication in a future issue of this journal, but has not been fully edited. Content may change prior to final publication. Citation information: DOI 10.1109/TIM.2019.2918372, IEEE Transactions on Instrumentation and Measurement

output consists of the digital timing signals indicating the distance measured and the echo pulse width and rise time. The key performance characteristic of the circuitry is its ability to detect the time position of the received nanosecond-scale echo pulse accurately, with a timing walk error of <1 cm (~70 ps), within a wide dynamic range of echo amplitudes (>1:10,000) and with a high single shot precision of ~200 ps (SNR~10), enabling high measurement speed limited by the pulsing rate of the laser diode transmitter (e.g. 100 kHz). The usability of the chip set and the attainable system level performance are demonstrated in a fully characterized pulsed TOF laser radar system. The key advantage of the presented chip set over prior art, e.g. in comparison to [14], is the substantially improved residual timing walk performance, which is achieved using the proposed time domain walk error compensation scheme based on a high performance multi-channel time-to-digital converter realization.

It is believed that the receiver-TDC chip set developed here could pave the way for the development of miniaturized low-power multi-channel laser radars that could enable the high speed measurement of 2-D and 3-D laser range images using 1-D and 2-D detector arrays.

The paper is organized as follows. Section II addresses the key design principles of a pulsed TOF laser radar and the details and performance of the receiver and TDC CMOS realizations developed here. The laser radar platform developed here and the system level measurements obtained are given in Sections III and IV, respectively. Conclusions and comparisons with previous studies are given in Section V.

II. Pulsed TOF Rangefinding Techniques

A. Basic Operation and Design Principles

Pulsed TOF laser radar techniques are based on sending short, intense laser pulses towards the target and measuring the time taken for them to travel to the target and back to the receiver. In general, high-power pulsed LDs must be used in order to achieve a measurement range of several tens of metres for Lambertian-type targets with a typical receiver aperture size (e.g. 2 cm in diameter). A shorter laser pulse will obviously yield a higher single-shot precision. On the other hand, in a high-peak power regime (>10 W), the minimum laser pulse width is restricted to a few nanoseconds on account of the difficulty in generating a pulse-mode drive current in the necessary >10 A/ns regime with readily available electronic solutions [16].

In the present case we used a commercial LD (905D1S2J03Y, Laser Components) in the transmitter, and this was driven with a metal–oxide semiconductor (MOS) -based current transient generator giving a drive current with an amplitude and pulse width of ~8 A and 3 ns, respectively [17]. The pulsing rate of the transmitter was ~10 kHz in the experiments described below, but can be raised to 100 kHz if needed. The optical output of the LD, recorded with a 25 GHz optical measurement head, is shown in Fig. 4. The start signal acting as the reference signal for the multi-channel TDC is discriminated from the driving current of the LD.

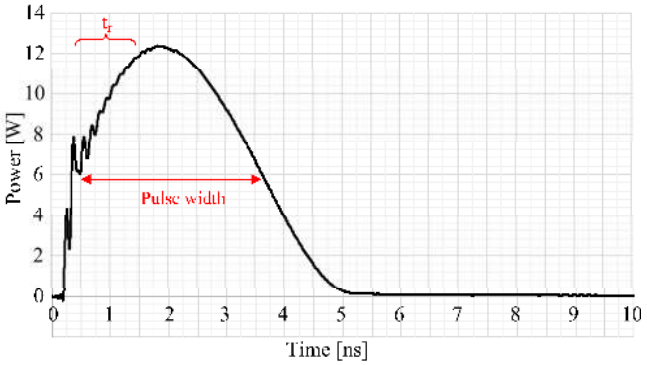

Fig. 4. Optical output pulse of the laser diode transmitter.

The half-value of the pulse width is approximately 3 ns, the wavelength 905 nm and the measured peak output power 18 W (12 W after the optics). Since the width of the pulse is ~3 ns (corresponding to a distance of approximately 1 m), it is obvious that simple threshold detection does not give the required centimetre-level accuracy, considering that the amplitude of the received echo may vary in a dynamic range of 1 to 10,000 or more.

The timing jitter of the measurement, i.e. the random variation of the measured distance, is determined by the signal-to-noise ratio [SNR, peak amplitude per root-mean-square (rms) noise] of the measurement. Assuming simple threshold detection and a receiver bandwidth matched to the rise of the laser pulse (i.e. with a rise time (t_r) of ~1.5 ns, a bandwidth of 230 MHz, ~0.35/t_r), the jitter is proportional to the ratio of the receiver noise to the slew rate of the timing signal [18]

$$\sigma_t = \frac{\sigma_{noise}}{\frac{d}{dt}[v(t)]_{t=t_p}} \approx \frac{t_r}{SNR} \text{ and } \sigma_R \approx \frac{t_r}{SNR} \times \frac{c}{2}, \quad (1)$$

where σ_t is the standard deviation of the timing jitter at the timing point t_p, σ_{noise} is the standard deviation of the receiver noise at the input to the timing comparator, $v(t)$ is the input signal of the timing comparator, and c is the velocity of the light. The jitter directly transforms to the single-shot range precision of the laser radar, σ_R. With a laser pulse rise time of 1.5 ns and a minimum SNR of ~7 (according to the desired false-alarm rate), the timing jitter for a single measurement is ~200 ps. The jitter is lower with a higher SNR and can be further improved by averaging several successive measurements.

The SNR can be calculated using the well-known radar equation. For a laser radar operating in a regime of geometrical optics (not diffraction-limited) and with non-cooperative Lambertian-type targets the power seen by the receiver is

$$P_r(R) = \frac{P_T \tau_T \rho A_r}{\pi R^2}, \quad (2)$$

where P_T is the peak pulsed output power of the LD, τ_T is the transmission of the optics, ρ is the reflection coefficient of a diffuse target, and A_r is the aperture of the receiver optics. With P_T = 12 W, τ_T = 0.7, ρ = 0.3, and a receiver aperture of 20 mm, for example, the received input power is approximately 25 nW

This article has been accepted for publication in a future issue of this journal, but has not been fully edited. Content may change prior to final publication. Citation information: DOI 10.1109/TIM.2019.2918372, IEEE Transactions on Instrumentation and Measurement

at a distance (R) of ~100 m. This corresponds to an APD output current of $i_{sig}(R) = P_r(R) \times R_0$, where R_0 is the responsivity of the APD. With R_0 = 40 A/W and P_r = 25 nW, the input current to the transimpedance amplifier (TIA) is ~1 µA. Assuming an input-referred current noise of ~100 nA for the receiver, an SNR of ~10 is achieved. This example calculation demonstrates that with these laser diode and system-level parameters a measurement range of ~100 m to non-cooperative targets is achievable with a single shot precision of ~3 cm (corresponding to a timing jitter of ~200 ps) and a high measurement speed of ~100 kHz…1 MHz (limited by the pulsing rate of the laser diode).

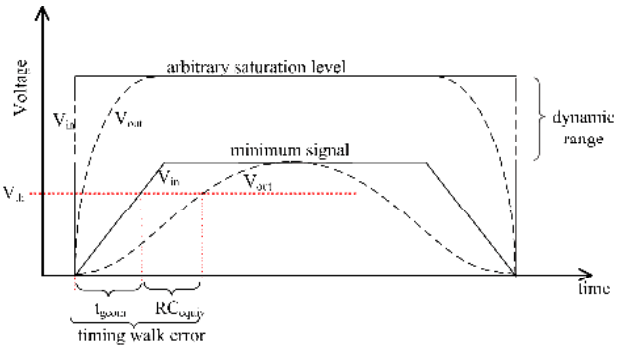

Fig. 5. Timing walk error in leading-edge detection.

B. Timing Discrimination and Walk Error

The main function of the receiver channel is to detect the time position of the weak optical echo pulse. This should be done accurately over the whole dynamic range of the received echo pulses from the minimum signal amplitude (SNR_{min}) up to the maximum (i.e. for the input current pulse range of ~1 µA…100 mA). In addition to the aforementioned random jitter due to the noise, the timing discrimination introduces a systematic timing-walk error, as already briefly discussed above.

The responses of the amplifier channel to small and large signals are shown in Fig. 5. In simple leading-edge detection with a constant threshold, one part of the error is produced by the finite rise time of the input pulse (geometrical error), denoted as t_{geom} in Fig. 5. With a rise time of 1.5 ns, for example, this error is ~750 ps, assuming that the minimum acceptable echo pulse amplitude is twice as high as the timing comparator threshold. Another source of timing-walk error is the varying electric delay of the receiver channel, denoted as RC_{equiv} in Fig. 5. For the maximum pulse (a step-like signal) this delay is almost negligible, while for the minimum signal it is equal to the equivalent RC time constant of the receiver, i.e. ~700 ps for a receiver bandwidth of ~200 MHz [14], [19]. Thus the total timing walk of the receiver within its dynamic range is approximately 1.5 ns with the aforementioned parameters. This is equivalent to a distance measurement error of ~25 cm without any corrective measures.

The timing-walk compensation is realized here in the time domain, using a multi-channel TDC. In the timing detection two parallel timing comparators with separate threshold voltages (V_{th_L} and V_{th_U}) are used, as shown in Figs. 3(b) and 6, three timing marks are discriminated — that from the lower threshold at the rising edge (stop1), that from the upper threshold at the rising edge (stop2), and that from the falling edge of the received pulse (stop3) at the lower threshold — as shown in Fig. 3(b). The multi-channel TDC then records the corresponding time intervals (start-stop1, stop1-stop2 and stop1-stop3) and this information is used for distance determination and time-domain walk error compensation.

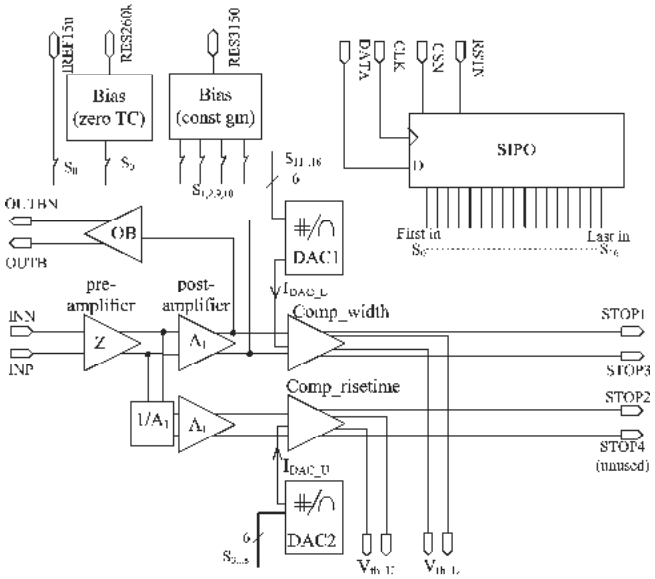

Fig. 6. Block diagram of the receiver channel.

C. Receiver Channel

The receiver channel, as shown in Fig. 6, was implemented in standard 0.35-µm CMOS technology [20]. The receiver-channel electronics consist of a transimpedance pre-amplifier, a voltage-type post-amplifier, two parallel timing comparators and bias circuitry. The current signal received from the APD is first amplified by the transimpedance-type pre-amplifier and then further amplified by post-amplifiers. Three timing signals (stop1, stop2, and stop3) are produced by using two parallel timing comparators: (Comp_width) produces a stop1 signal when the input crosses a programmable threshold (V_{th_L}), and the upper threshold voltage (V_{th_U}) is used for the parallel timing comparator (Comp_risetime), which produces a second timing mark (stop2). Finally, a third timing signal is produced when the trailing edge falls below the V_{th_L} of the (Comp_width) comparator. The reference voltages for the timing comparators are set by adjusting the currents I_{DAC_L} and I_{DAC_U}. V_{th_L} for the (Comp_width) and V_{th_U} for the (Comp_risetime) can be adjusted using 6-bit DACs with LSBs of 2.7 and 15.7 mV, respectively. The receiver also includes readout circuitry for the threshold voltages.

The measured characteristics of the receiver channel are as follows: transimpedance ~100 kΩ, bandwidth ~250 MHz, input-referred rms noise current of the receiver ~100 nA ($C_{in,total}$~ 3 pF), and power consumption approximately 180 mW. The walk measurement showed that the original timing-walk error at the level of 2.5 ns was reduced to ±25 ps (±4 mm in distance) over a dynamic range of ~ 1:100,000 using

This article has been accepted for publication in a future issue of this journal, but has not been fully edited. Content may change prior to final publication. Citation information: DOI 10.1109/TIM.2019.2918372, IEEE Transactions on Instrumentation and Measurement

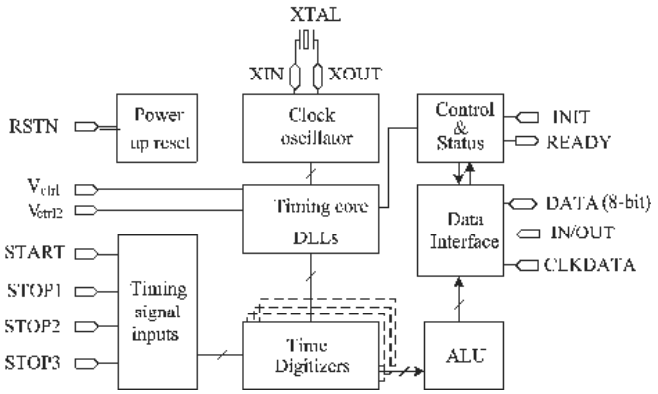

Fig. 7. Block diagram of the time-to-digital converter.

the proposed time-domain walk error compensation techniques. The size of the layout of the receiver channel is approximately 2 mm × 2 mm, and it is enclosed in a QFN36 package.

D. Time-to-Digital Converter

A multi-channel TDC, the operation principle, construction and performance parameters of which are presented in detail in [21], is composed of the blocks shown in Fig. 7. Its operation is based on a 7-bit counter and two-level stabilized delay line interpolation. The TDC solves the time intervals (Δt_1, Δt_2, Δt_3) accurately between the start and the three timing signals (stop1, stop2, stop3) received from the receiver IC. The reference start signal, which indicates the beginning of the measurements, is taken electrically from the driving current of the LD transmitter. Start–stop1 (Δt_1) defines the actual distance information, including the walk error. Stop1-stop3 (Δt_2) determines the width of the measured pulse, and stop1–stop2 (Δt_3) corresponds to the rise time of the measured pulse, for use in walk error compensation.

The multi-channel TDC implemented in a standard 0.35-µm CMOS technology achieves a timing resolution (σ_{rms}) of <10 ps and a measurement range of 530 ns, corresponding to a distance of ~80 m. The delay locking stabilizes the measurement against process, voltage and temperature variations. Its supply voltage is 3.3 V, and the power consumption is ~150 mW. The size of its IC is 2.5 mm × 4 mm, and it is enclosed in a plastic QFN48 package.

III. Characterization Platform

The use of the receiver-TDC chip set developed here was demonstrated on specially constructed a laser radar platform. The system, depicted in Fig. 8, consists of a laser diode transmitter, paraxial optics and the receiver electronics, including an APD detector (First Sensor,AD230-8 TO52S1) and the receiver–TDC chip set, as presented above. The laser radar was controlled by a Xilinx Spartan6 FPGA processor (OpalKelly XEM6001) using Verilog code on a development platform. The computer-connected control system was driven by means of Python-based measurement software.

The optics used in the laser radar are shown in Fig. 9. The receiver uses paraxial optics, and the focal lengths of the transmitter and receiver optics are 30 and 20 mm, respectively.

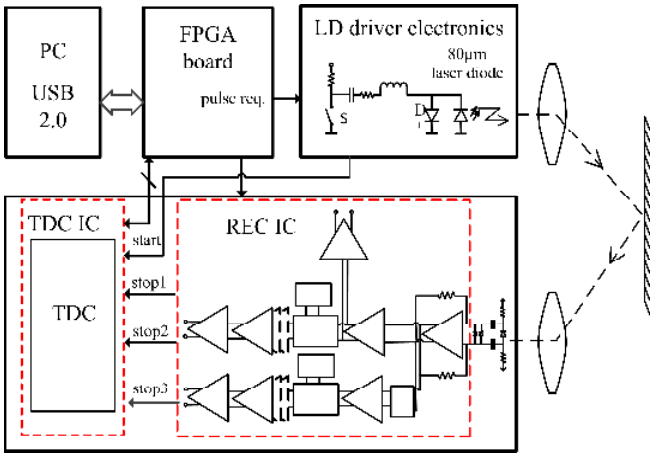

Fig. 8. Block diagram of the laser radar.

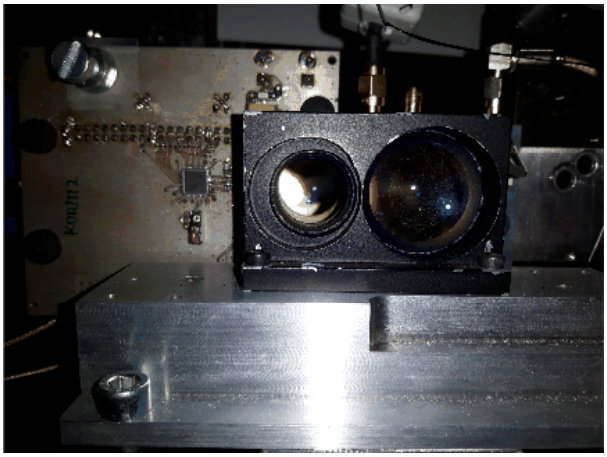

Fig. 9. Paraxial optics.

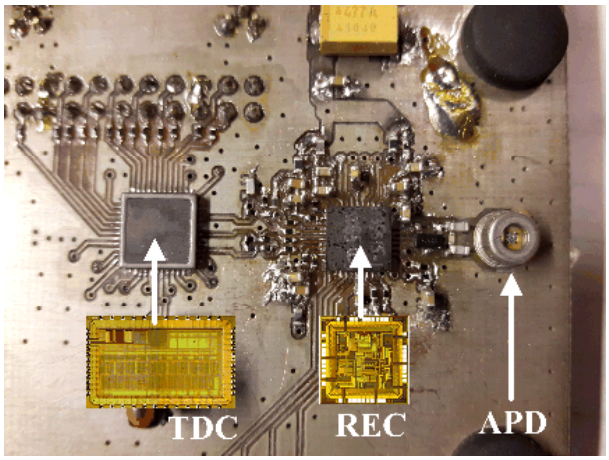

Fig. 10. Measurement PCB, including an avalanche photodiode, a receiver IC, and a TDC IC.

The aperture of the receiver lens is 20 mm, and the width of the emitting stripe of the LD is 80 µm. This corresponds to a divergence of the laser beam (θ_t) of ~2.7 mrad, yielding a spot size of 8 cm at 30 m. The receiver electronics, including the APD, receiver channel and TDC, were installed on a single printed circuit measurement board (PCB), as shown in Fig. 10.

This article has been accepted for publication in a future issue of this journal, but has not been fully edited. Content may change prior to final publication. Citation information: DOI 10.1109/TIM.2019.2918372, IEEE Transactions on Instrumentation and Measurement

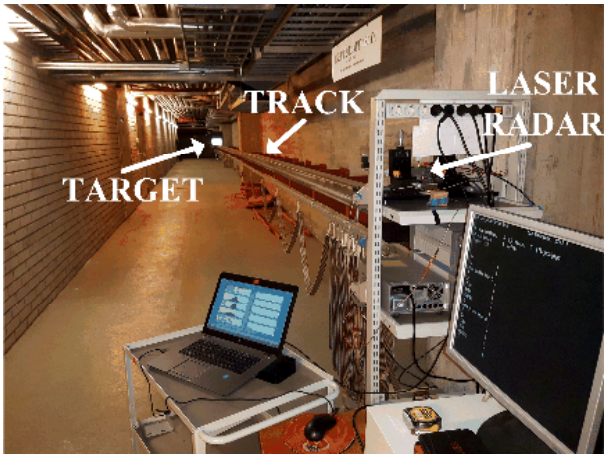

Fig. 11. Pulsed TOF measurement track.

IV. Measurement Results

The TOF measurements were performed using the calibrated automated linearity measurement track shown in Fig. 11. This had an estimated target-locating accuracy of ±0.3 mm, and the target distance was varied within a range of 3 to 34 m (maximum operation range for the track). The background radiation level during the measurements was <50 lx (normal laboratory conditions).

Three kinds of target material differing in their reflectivity were used to alter the level of the input signals. For example in [13] different reflectance coefficients (ρ) were given for different materials at 900 nm wavelength. Here, a calibration measurement was done for measuring reflectance properties of target materials such as black cardboard (reflectivity $\rho \approx 0.12$), white paper ($\rho \approx 1$), and a mirror-like reflective sheet ($\rho >> 1$). An input signal level of SNR ≈ 50 was received with the measurement track at its maximum length (34 m) and using the black cardboard as a target. Since the amplitude of the received echo signal decreases proportionally to the second power of distance, a maximum distance from this target can be estimated to be ~100 m (SNR~5). At the other extreme, the input amplitude started to decrease at distances shorter than 5.5 m owing to the parallel optics used in the laser radar, and since the receiver sees only a small portion of the light spot on the target at short distances, the signal was too weak for measurement at less than 3 m. The effect of the target distance on the dynamic range of the optical input signal was ~1:38 (at distances of 3–34 m). As a result, the total dynamic range of the optical input signal amplitude was approximately 1:40,000 when different target surfaces were used in the linearity measurements (at distances of 3–34 m).

The lower threshold voltage (V_{th_L}) was set to correspond to approximately 7 times the RMS-noise value (electrical noise) at the input to the timing comparator (Comp_width in Fig. 6). The upper threshold (V_{th_U}) was set to correspond to approximately 50 times the RMS noise value at the input of the parallel timing comparator (Comp_risetime in Fig. 6). The exact value of the upper threshold voltage is not critical as far as timing-walk compensation is concerned. It is only important to use the same threshold voltages for the calibration measurement (for constructing the compensation tables) and for the actual distance measurements for which the tables are used.

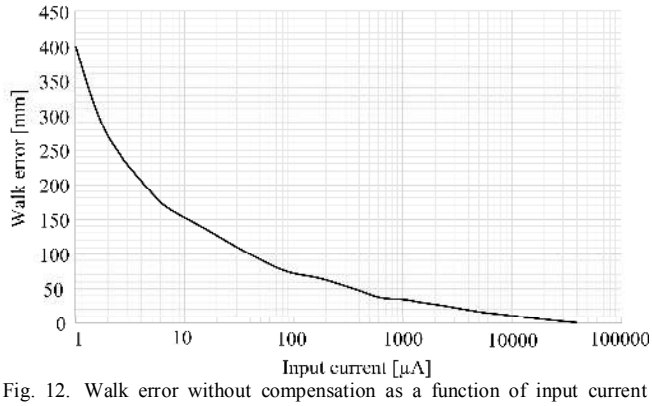

Fig. 12. Walk error without compensation as a function of input current amplitude.

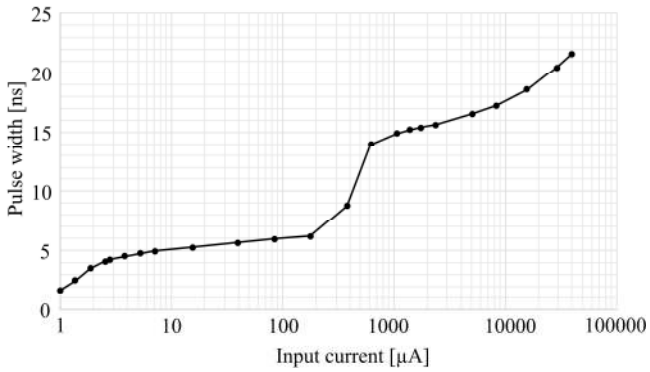

Fig. 13. Measured pulse width as a function of input amplitude.

A. Calibration Measurements

The calibration measurements were carried out at a fixed distance and with a variable optical neutral density filter (ND) used in front of the transmitter lens to sweep the input amplitude over the dynamic range of ~1:40,000 (the same as the signal range in the linearity measurements). The multi-channel TDC was then used to measure the time intervals between the start signal and the three timing marks stop1, stop2, and stop3. The measured timing-walk error without compensation is shown as a function of input current amplitude in Fig. 12. The resulted walk error was approximately 40 cm, which is 2.8 ns in time, over the amplitude range from ~1 μA–40 mA.

The width of the measured echo pulse as a function of the input current from the APD is shown in Fig. 13, where the pulse width is seen to increase monotonically with an increasing APD current. Thus this information can be used for timing-walk error compensation.

Two compensation curves were generated. In Fig. 14 the measured uncompensated timing-walk error (change in the timing moment at the lower threshold (V_{th_L}) due to the varying input amplitude) is shown as a function of the measured pulse width (stop1-stop3), containing 116 measurement points. The measured pulse width widened monotonously from ~1.5 to 22 ns as the input signal level was increased.

This article has been accepted for publication in a future issue of this journal, but has not been fully edited. Content may change prior to final publication. Citation information: DOI 10.1109/TIM.2019.2918372, IEEE Transactions on Instrumentation and Measurement

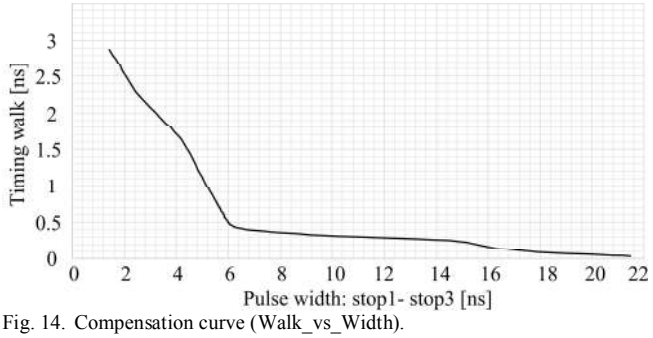

Fig. 14. Compensation curve (Walk_vs_Width).

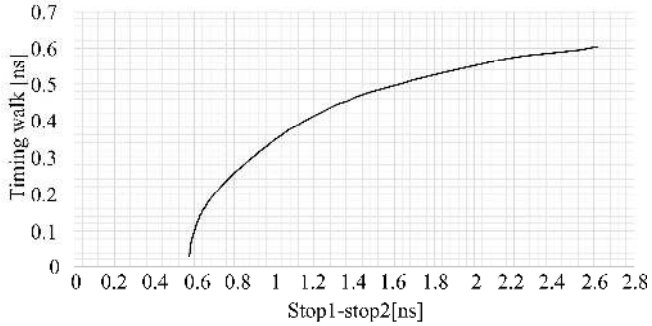

Fig. 15. Compensation curve (Walk_vs_Risetime).

The stop2 signal is sent from the receiver IC as the input signal reaches an SNR level of ~500, whereupon the behaviour of the timing error as a function of Δt_{rise} (stop1–stop2) is as shown in Fig. 15. Note that the operation range of the rise time measurement is limited to signal amplitudes exceeding the upper threshold only.

B. *Single-Shot Measurements*

Single-shot measurements were performed at a distance of 34 m. The measurements were repeated 5,000 times, and each of the individual results was automatically corrected by reference to the Walk_vs_Width compensation curve shown in Fig. 14.

The distributions of the 5,000 single-shot compensated measurement results obtained at a distance of 34 m for different target materials using the Walk_vs_Width timing-walk compensation method are shown in Fig. 16. As is seen, the single shot precision is ~36mm (sigma value) with an SNR of ~10 and improves to about ~2 mm at higher signal amplitudes. Note also that the average of the distributions remains at 34 m even though the signal level varies considerably.

C. *Accuracy and Linearity Measurements*

The linearity error was measured using a calibrated track, as shown in Fig. 11, and sweeping the distance from the target from 3 to 34 m in 0.5–1-m steps. Black cardboard (black lines), white paper (blue lines), and a diamond-grade sheet (red and orange lines) were used as targets. In addition, to achieve the SNR_{min} signal level, an extra ND filter with a transmittance of 21% was included when the black cardboard was used (green line). As a result, the reflected power varied within a range of approximately 1:40,000 owing to the distance variation and the target reflectance properties.

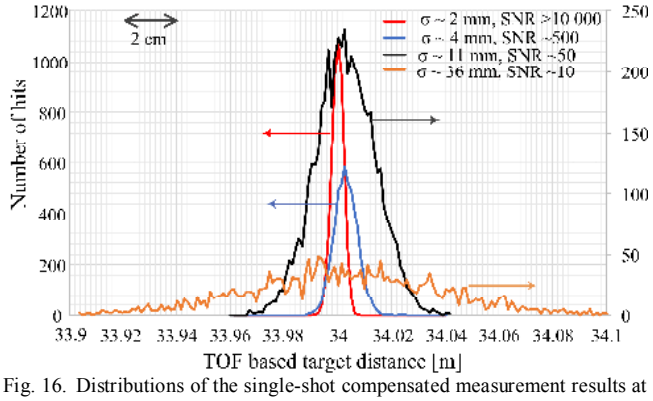

Fig. 16. Distributions of the single-shot compensated measurement results at 34 m; red ($\rho >> 1$), blue ($\rho \approx 1$), black ($\rho \approx 0.12$), orange [$\rho \approx 0.12$ + ND filter (21% transmittance)].

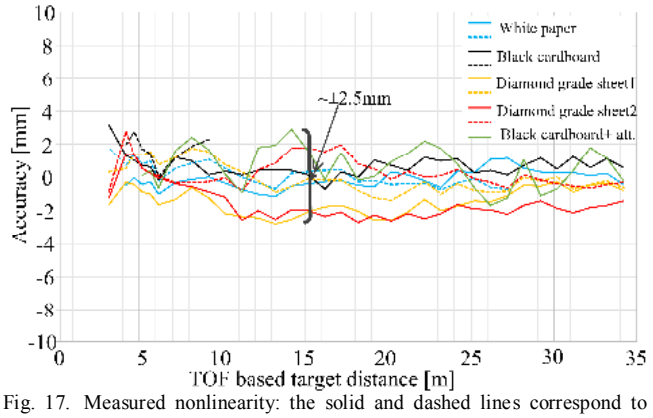

Fig. 17. Measured nonlinearity: the solid and dashed lines correspond to Walk_vs_Width and Walk_vs_Risetime, respectively, and the measured total amplitude variation is approximately 1:40,000.

5,000 individual measurements were averaged at each distance and the timing-walk errors were subtracted from the measured distance results by determining the corresponding walk error using either the Walk_vs_Width or Walk_vs_Risetime compensation curve in the calibration, as shown in Figs. 14 and 15. The resulting linearity errors for the different target surfaces are shown in Fig. 17 as a function of the reference distance. The solid lines depict the compensated distance results obtained using the measured pulse width, and the dashed lines indicate compensated measurement results based on Walk_vs_Risetime compensation. As shown, the accuracy is better than ±2.5 mm over the dynamic range of 1:40,000.

D. *Temperature Measurements*

The temperature drift was measured by placing the laser rangefinding receiver board shown in Fig. 10, excluding the optomechanical head and transmitter, in a temperature cabin and measuring the compensation curves (Walk_vs_Width and Walk_vs_Risetime) at temperatures ranging from –30 to +78 ˚C. The temperature measurements were performed over an input dynamic range of ~1:2,600. The objective was to explore what accuracy would be achieved if the compensation curves measured at 22˚C only were used for all temperatures (range –

This article has been accepted for publication in a future issue of this journal, but has not been fully edited. Content may change prior to final publication. Citation information: DOI 10.1109/TIM.2019.2918372, IEEE Transactions on Instrumentation and Measurement

TABLE I
PERFORMANCE SUMMARY AND COMPARISON OF RECENTLY PUBLISHED RECEIVERS

	This work	[14]	[23]	[24]	[25]	[26]	[27]
Technology	**CMOS 0.35 µm**	BiCMOS 0.8 µm	CMOS 0.18 µm	CMOS 0.13 µm	CMOS 0.35 µm	CMOS 0.18 µm	CMOS 0.18 µm
Bandwidth	**230 MHz**	250 MHz	720 MHz	640 MHz	140 MHz	150 MHz	110 MHz
Type of receiver	**Rx TDC chip set**	Rx+ external TDC	Rx	Rx	Rx	Rx	Rx
Input-referred current noise	**~100 nA**	~110 nA	170 nA	120 nA	19 nA *	56 nA	23nA
Gain control	**not needed**	yes	yes	yes	yes	yes	yes
Laser radar measurements	**yes**	yes	yes	NA	NA	NA	NA
Dynamic range	**>1:40,000**	1:4000	1: 12,000	1:1600	1:12,000	1:2000	1:2000
Accuracy @ 22°C	**± 2.5 mm**	± 35mm	NA	NA	± 210 mm	± 149 mm	NA
Temp range	**-30 to +80 °C**	0 to +50 °C	NA	-10 to +60 °C	-40 to +85 °C	NA	NA
Temp dependence	**~± 10 mm**	NA	NA	NA	± 210mm to ± 240mm	NA	NA
Precision	**36 mm @SNR= 10**	9.5mm @SNR 35	NA	NA	NA	NA	NA
(*) integrating mode, with 5 ns staircase pulse							

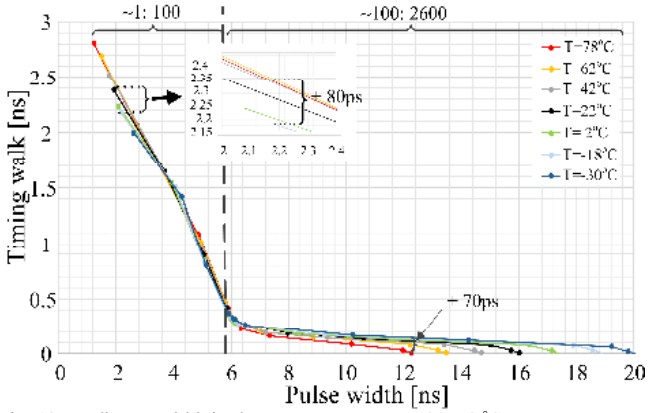

Fig. 18. Walk_vs_Width in the temperature range -30–78 ˚C.

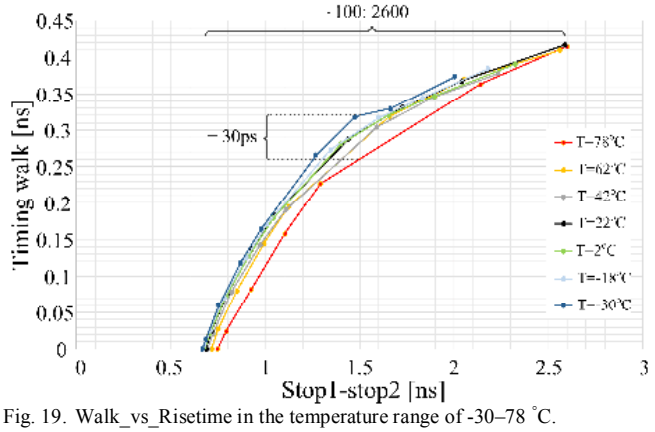

Fig. 19. Walk_vs_Risetime in the temperature range of -30–78 ˚C.

30 to +78 ˚C). Compensation curves (Walk_vs_Width) measured at several temperatures are depicted in Fig. 18. As shown, the maximum error due to temperature variation (difference between the measured curves at various temperatures) is approximately ±80 ps (±12 mm) for the compensated measurement result in a dynamic range of 1:100, which corresponds to the linear range of the receiver channel. In the range 100:2,600 the error is approximately ±70 ps (±10.5 mm).

The Walk_vs_Risetime compensation curves measured at several temperatures (ranging from –30 to +78 ˚C) are shown in Fig. 19. The maximum error within the dynamic range 100: 2,600 is approximately ±30 ps (±4.5 mm), which is considerably better than the result for compensation based on pulse-width measurement in the same dynamic range. The reason for this behaviour is that the width behaviour is more temperature-dependent in this range owing to the receiver input parameters (operation of protection diodes, RC time constants, operation of pre-amplifier), for example. Stop2 is nevertheless generated by the rising edge of the pulse, which is still in the linear range of the preamplifier and is thus more stable as a function of temperature.

V. CONCLUSIONS

A receiver–TDC chip set was developed, implemented in 0.35-µm CMOS technology and tested in a pulsed TOF laser rangefinder platform. Millimetre-level accuracy was achieved by means of time-domain walk error compensation techniques, which have the advantage of also working for clipped receiver pulses. For this reason, the narrow linear range which is typical of low-noise optical receivers does not restrict the permitted dynamic range of the input optical echo pulse.

The nonlinearity of the distance measurement is better than ±2.5 mm within a range of 3 to 34 m (maximum range limited by the length of the track), as measured with different types of target corresponding to an input dynamic range of ~1:40,000. The single-shot precision is better than 36 mm at an SNR of ~10, ~10 mm at an SNR of ~50 and ~2 mm at an SNR of >10,000. The temperature drift of the measurement is approximately ±1 cm within the temperature range –30 to +80 ˚C.

Pulsed TOF laser radar techniques are widely used,

especially in laser scanning applications [10], [22], and current laser scanners are typically based on mechanical scanning of the laser beam over the region of interest. The current research trend, however, is towards the development of solid-state scanners, e.g. by using the focal plane scanner approach, where a 1-D or 2-D array of detectors is located on the focal plane of the receiver optics [23]. In this case miniaturization of the lidar electronics is essential in order to reduce the complexity of the system. This study has shown that in principle it is possible to realize the high performance receiver and multi-channel TDC of a pulsed TOF laser radar on a single CMOS die with state-of-the art system-level performance.

The performance of the measured chip set is summarized and compared with recently published works within this field in Table I. It should be noted however, that most of the prior studies in this field (e.g. [23]–[27]) have focused mainly on the development of an integrated receiver for a pulsed TOF laser radar without complete characterization of the device at the system level nor concurrent time-to-digital converter development. In [25]–[26], the timing accuracy is less than ±75 mm within a dynamic range of approximately <1:10,000, whereas millimetre-level accuracy was achieved over a wider dynamic range in the present study, however at a cost of somewhat higher noise. A complete receiver TDC chip set was developed in [14] but the dynamic range and accuracy are worse with a factor of ~10 compared to the present design.

The feasibility of the developed circuits and timing-walk error compensation techniques were demonstrated using a laser radar platform. Since both functionalities are based on the same non-aggressive CMOS technology, they can in principle be realized on the same die, which could pave the way for miniaturized laser radar sensor and scanner systems.

REFERENCES

[1] J. Kostamovaara, K. Määttä, and R. Myllylä, "Pulsed time-of-flight laser rangefinder techniques for industrial applications," in *Proc. SPIE Conf. Intell. Robot. Systs.*, vol. 1614, pp. 283–295, Nov. 1991.

[2] I. Kaisto, J. Kostamovaara, I. Moning, and R. Myllylä, "Laser rangefinding techniques in sensing of 3-D objects," in *Proc. SPIE*, Santa Clara, CA, vol. 1260, pp.122–133, 1990.

[3] C. Mallet and F. Bretar, "Full-waveform topographic lidar: state-of-art," *ISPRS J. Photogram. Remote Sens.*, vol. 64, no. 1, pp.1–16, Jan. 2009.

[4] C. S. Bamji *et al.*, "A 0.13 µm CMOS system-on-chip for a 512x 424 time-of-flight image sensor with multi-frequency photo-demodulation up to 130 MHz and 2 GS/s ADC," *IEEE J. Solid-State Circuits*, vol. 50, no. 1, pp. 303–319, Jan. 2015.

[5] M.-C. Amann, T. Bosch, M. Lescure, R. Myllylä, and M. Rioux, "Laser ranging: A critical review of usual techniques for distance measurement," *Opt. Eng.*, vol. 40, no. 1, pp. 10–19, 2001.

[6] R. Lange, P. Seitz, A. Biber, and S. Lauxtermann, "Demodulation pixels in CCD and CMOS technologies for time-of-flight ranging," *Proc. SPIE*, vol. 3965A, San Jose, CA, pp. 177–188, Jan. 2000.

[7] O. Shcherbakova, L. Pancheri, G.-F. Dalla Betta, N. Massari, and D. Stoppa, "3D Camera based on linear-mode gain-modulated avalanche photodiodes," in *Proc. IEEE Int. Solid-State Circuits Conf. Dig. Tech. Papers (ISSCC)*, San Francisco, CA, USA, Feb. 2013, pp. 490–491.

[8] K.-H. Thiel and A. Wehr, "Performance capabilities of laser scanners–An overview and measurement principle analysis," in *Proc. ISPRS Workshop*, Freiburg, Germany, pp. 14–18, Oct. 2004.

[9] B. Schwarz, "LIDAR: Mapping the world in 3D," *Nat. Photon.*, vol. 4, no. 7, pp. 429–430, Jul. 2010.

[10] R. Halterman and M Brunch, "Velodyne HDL-64E lidar for unmanned surface vehicle obstacle detection", *in Proc. SPIE*, Orlando, Florida, vol 7692, pp. 644–651, April 2010.

[11] Y. Tang *et al.*, "Vision-aided multi-UAV autonomous flocking in GPS-denied environment," *IEEE Trans. on Industrial Electronics*, vol. 66, no. 1, pp. 616-626, Jan. 2019.

[12] RCA Corporation, Electro-Optics Handbook, tech. ser. EOH-11, RCA, Inc., Lancaster, Pa., 1974.

[13] Riegl, Riegl laser measurement systems, application note AN- GI0002, Riegl, USA URL: http://riegl.com/uploads/tx_pxpriegldownloads/General-Information-Distancemeter.pdf

[14] P. Palojärvi, T. Ruotsalainen, and J. Kostamovaara, "A 250-MHz BiCMOS receiver channel with leading edge timing discriminator for a pulsed time-of-flight laser rangefinder," *IEEE J. Solid-State Circuits*, vol. 40, no. 6, pp. 1341–1349, Jun. 2005.

[15] T. Ruotsalainen, P. Palojärvi, and J. Kostamovaara, "A wide dynamic range receiver channel for a pulsed time-of-flight laser radar," *IEEE J. Solid-State Circuits*, vol. 36, no. 8, pp. 1228–1238, Aug. 2001.

[16] S. N. Vainshtein, V. S. Yuferev, and J. Kostamovaara, "Avalanche transistor operating at extreme currents: physical reasons for low residual voltages," *Solid-State Electron.*, vol. 47, no. 8, pp. 1255–1263, Aug. 2003.

[17] L. Hallman, J. Huikari, and J. Kostamovaara, "A high-speed/power laser transmitter for single photon imaging applications," *in Proc. IEEE Sensors Conf.*, Valencia, Spain, Nov. 2014, pp. 1157–1160.

[18] G. Bertolini and A. Coche, *Semiconductor Detectors*, Amsterdam, The Netherlands: North-Holland, 1968.

[19] R. J. van Plassche and P. Baltus, "An 8-bit 100-MH full-Nyquist analog-to-digital converter," *IEEE J. Solid-State Circuits*, vol. 23, no. 12, pp. 1334–1244, Dec. 1988.

[20] S. Kurtti, J. Nissinen, and J. Kostamovaara, "A wide dynamic range CMOS laser radar receiver with a time-domain walk error compensation scheme," *IEEE Trans. Circuits Syst. I, Reg. Papers*, vol. 64, no. 3, pp. 550–561, Mar. 2017.

[21] J. Jansson, A. Mäntyniemi, and J. Kostamovaara, "A CMOS time-to-digital converter with better than 10 ps single-shot precision," *IEEE J. Solid-State Circuits*, vol. 41, no. 6, pp. 1286–1296, Jun. 2006.

[22] P. Riegel and A Ullrich, "Resolving range ambiguities in high-repetition rate airborne light detection and ranging applications," J. Appl. Remote Sens., vol. 6, no. 1, pp. 063552-1–063552-18, Jul. 2012.

[23] C. Hong *et al.,* "A linear-mode LiDAR sensor using a multi-channel CMOS transimpedance amplifier array," *IEEE Sensors J.*, vol. 18, no. 17, pp. 7032–7040, Sep. 2018.

[24] T.-H. Ngo *et al.*, "Wideband receiver for a three-dimensional ranging LADAR system," *IEEE Trans. Circuits Syst. I, Reg. Papers*, vol. 60, no. 2, pp. 448–456, Feb. 2013.

[25] H.-S. Cho, C.-H. Kim, and S.-G Lee, "A high-sensitivity and low walk error LADAR receiver for military application," *IEEE Trans Circuits Syst. I, Reg. Papers*, vol. 61, no. 10, pp. 3007–3015, Oct. 2014.

[26] H. Zheng, R. Ma, M. Liu, and Z. Zhu, "A linear dynamic range receiver with timing discrimination for pulsed TOF imaging LADAR application," *IEEE Trans. Instrum. Meas.*, vol. 67, no. 11, pp. 2684–2691, Nov. 2018.

[27] R. Ma, M. Liu, H. Zheng, and Z. Zhu, "A 66 dB linear dynamic range, 100 dBΩ transimpedance gain TIA with high speed PDSH for lidar," *IEEE Trans. Instrum. Meas.*, early access, 2019.

Sami Kurtti was born in Kuusamo, Finland, in 1979. He received the M.Sc.Tech and Dr.Tech. degrees in electrical engineering from the University of Oulu, Finland, in 2004 and 2013, respectively. He was a research scientist from 2004 to 2013 and has been a Post-Doctoral Researcher with Circuits and Systems Research Unit, University of Oulu, since 2013. His interests include the development of analogue and mixed-signal integrated circuits and structures for pulsed time-of-flight laser rangefinders.

This article has been accepted for publication in a future issue of this journal, but has not been fully edited. Content may change prior to final publication. Citation information: DOI 10.1109/TIM.2019.2918372, IEEE Transactions on Instrumentation and Measurement

Jussi-Pekka Jansson received the degrees of Dipl.Eng. and Dr.Tech in electrical engineering and title of Adjunct Professor in 2004, 2012 and 2017, respectively, all from the University of Oulu, Finland. He works as a post-doctoral researcher at the same University, with the Circuits and Systems research unit. His research interests include high precision time-to-digital converter architectures and applications related to them.

Juha Kostamovaara (M'85, S'13) received the Dr. Eng. (electrical engineering) degree from the University of Oulu, Oulu, Finland, in 1987. Kostamovaara has hold the Academy professorship position funded by the Academy of Finland during 2006 - 2017. Currently he holds a professorship in electronics at the University of Oulu (Circuits and Systems Research Unit). His main research interest is in the development of pulsed time-of-flight devices, circuits and systems for electronic and optoelectronic measurements.